THE ASTROPHYSICAL JOURNAL, 471:L53–L56, 1996 November 1

A MECHANISM FOR THE PRODUCTION OF JETS AND ANSAE IN PLANETARY NEBULAE

ADAM FRANK,[1] BRUCE BALICK,[2] AND MARIO LIVIO[3]
Received 1996 June 3; accepted 1996 August 22

ABSTRACT

Many elliptical planetary nebulae (PNs) exhibit pairs of small, low-ionization structures called "jets" and ansae, which are characterized by their equal and opposite displacements (0.01–0.03 pc) and redshifts (50 km s^{-1}) from the nucleus along the nebular symmetry axis. Here we propose that jets and ansae can quite easily develop prior to the onset of the fast wind during the proto-PN phase. Using nominal descriptors, which include an accelerating fast wind and a toroidal slow-wind mass-loss geometry to form elliptical PNs, we find a wide range of conditions under which jets and ansae can develop. We show that the expected sizes, velocities, and ionization of these microstructures conform quite nicely to observations.

Subject headings: circumstellar matter — ISM: jets and outflows — planetary nebulae: general

1. INTRODUCTION

The general properties of elliptical planetary nebulae (EPNs; Balick 1987) have been very successfully explained by a class of hydrodynamic models known as interacting stellar winds (ISW). In the ISW scenario, fast winds (1000 km s^{-1}) sweep into older material ejected during the previous slow-wind phase (10–20 km s^{-1}). A hot interior bubble forms whose expansion drives a thin, dense "snowplow" supersonically into the downstream, undisturbed slow wind (Kwok, Purton, & Fitzgerald 1978; Kahn 1983; Marten & Schoenberner 1991; Frank 1994; Mellema 1994).

Balick (1987) conjectured that if the slow wind was ejected as a relatively dense torus, then the bubble would expand fastest along the nebular symmetry axis, generating a prolate EPN. Detailed analytical and numerical hydrodynamic models (Balick, Preston, & Icke 1987; Soker & Livio 1989; Mellema, Eulderink, & Icke 1991; Icke, Balick, & Frank 1992; Frank et al. 1993; Dwarkadas, Chevalier, & Blondin 1996) have explored this mechanism and its efficacy. Two of the key parameters determining the shape of the EPN are q, the ratio of equatorial to polar densities, and, to a lesser degree, the initial velocity of the slow wind.

PNs also contain a variety of microstructures (cf. Balick 1987) whose origins have remained puzzling. Some of the most striking and enigmatic of these are pairs of low-ionization knots, or "ansae" (Aller 1941), and collimated outflows, or "jets," lying along the polar axis of many EPNs. Many of the microstructures are "FLIERs" (Balick et al. 1993, 1994), which are characterized by highly supersonic motions (35–70 km s^{-1}) through the medium in which they appear embedded. In some cases, FLIERs appear to have the same thermal pressures as their immediate surroundings, suggesting that any confinement is the result of external ram pressure. Also, spectroscopic observations by Balick et al. (1993, 1994) seemingly conflict with the expectation that bow shocks should form as the FLIERs burrow into the surrounding nebula.

Hydrodynamic models have also failed to explain the jets and ansae in EPNs (Mellema 1996). At the high speeds of the fast winds, $v_{\rm fw}$, most windblown bubbles in PNs are "energy conserving" (Dyson & Williams 1980), meaning that the kinetic energy of the winds is thermalized at $T \approx \frac{3}{16} m_p v_{\rm fw}^2 / k \sim 3 \times 10^7$ K. Radiative cooling rates are so low that the bubbles remain large and hot even as they expand with very high sound speeds ($\approx 0.3\, v_{\rm fw}$). Under these conditions, collimated thick supersonic jets *can* form inside the hot bubble (Icke et al. 1992; Frank & Mellema 1994). However, owing to their high internal pressure, the flows of the fast winds do not converge to form stable, low-ionization microstructures like ansae, thin jets, and FLIERs.

Here we consider whether the highly successful ISW models of PNs might be applied to the evolution of proto-EPNs (PPNs) in order to understand the formation of ansae and jets. We show that such flows will naturally occur in momentum-conserving PPN bubbles, and that they can naturally account for the formation of jets and ansae in a way consistent with extant observations.

2. MODEL

Overview.—First, we recognize that the change in wind character from slow to fast occurs gradually. This is crucial. As Kahn & Breitschwerdt (1990; hereafter KB) recognized, the shocks formed as winds collide will be fully radiative so long as the interaction between them occurs at velocities below 160 km s^{-1}. At these speeds, the heat generated by the wind's kinetic energy is efficiently converted into escaping radiation. This means that proto-PNs will be "momentum-conserving" windblown bubbles that develop a dense sheet of compressed gas between the wind upstream and the older, undisturbed (slow-wind) gas downstream.

Any equator to pole density contrast in the slow wind will result in a prolate geometry for the shocks (Fig. 1 [Pl. L4]). Wind streamlines will become axisymmetric as the wind encounters the inner shock obliquely. Upon crossing the inner shock, the normal component of motion is sharply reduced. On the other hand, the tangential component is unchanged across the shock. This forces the streamlines to become "refracted." The decelerated wind flows essentially parallel to the shock, whence the gas slides along the shock's prolate boundary (the contact discontinuity) toward the symmetry axis.

Assuming that the prolate shock does not change its shape,

[1] Hubble Fellow: Department of Astronomy, University of Minnesota, Minneapolis, MN 55455; afrank@s1.msi.umn.edu.
[2] Department of Astronomy, University of Washington, P.O. Box 351580, Seattle, WA 98195; balick@astro.washington.edu.
[3] Space Telescope Science Institute, Baltimore, MD; mlivio@stsci.edu.

PLATE L4

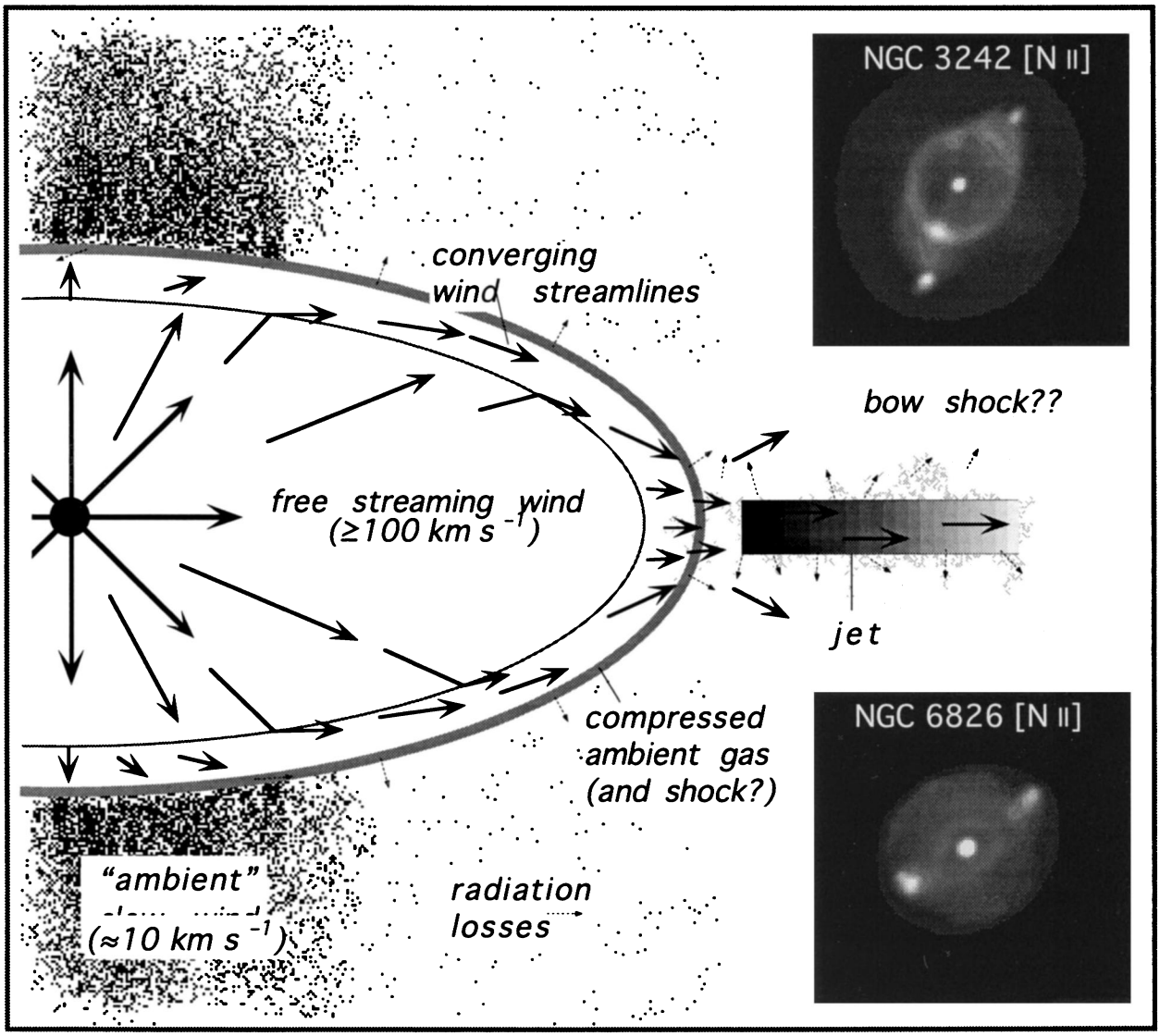

FIG. 1.—Schematic for the production of jets and ansae in PN. Two [N II] images of the elliptical PN with ansae are also shown.

FRANK, BALICK, & LIVIO (see 471, L53)

the gas flows converge at the axis where they collide, forming a new shock that redirects the flow into a jet moving outward along the long axis of the bubble in a manner described by Cantò, Tenorio-Tagle, & Różyczka 1988, hereafter CTTR (cf. Mellema 1996). In a second paper, Tenorio-Tagle, Cantò, & Różyczka (1988) numerically simulated the evolution of conically converging flows, demonstrating that classical supersonic jets are effectively formed. More recently, Mellema & Frank (1996) have observed conically converging flows forming jets in models of young stellar object windblown bubbles.

If the system grows and/or changes its shape, the convergent point for the flows can change. This can produce several types of morphologies for the jets and ansae.

Once the accelerating stellar winds pass the 160 km s^{-1} velocity threshold, cooling becomes inefficient. An "energy-conserving" (nonradiative) hot bubble quickly develops behind the compressed sheet. Flows now converge inside the hot bubble, and the high sound speed in the hot bubble acts quickly to suppress the formation of any density inhomogeneities. Thus, the era of dense, low-ionization jet and ansa formation comes to a close.

Bubble dynamics.—To begin our calculation, we must assume a functional form for the evolution of the fast wind as the central star temperature rises. We will follow the formalism of KB and assume that the fast wind evolves in such a way that its total momentum input ($\dot{\Pi}$) is constant ($\dot{\Pi} = \dot{M}_{\rm fw} V_{\rm fw} = {\rm const}$). For simplicity, we chose a simple power law for the evolution of both the velocity and the mass-loss rate of the fast wind:

$$\dot{M}_{\rm fw}(t) = \dot{M}_{\rm fw0}(t_0/t)^n, \quad V_{\rm fw}(t) = V_{\rm fw0}(t/t_0)^n, \tag{1}$$

where t_0 is the time at which the fast wind begins. We also assume that the slow wind was ejected with a constant mass-loss rate $\dot{M}_{\rm sw}$, velocity $V_{\rm sw}$, and pole to equator density contrast ($q = \rho_E/\rho_P$).

In their work on PNs and accelerating winds, KB demonstrated that the shell expands with constant velocity during the momentum-conserving phase. During this period, the expansion of the bubble can be written as $r_s = (1 + \sqrt{\alpha}) v_{\rm sw} t$, where $\alpha = \dot{M}_{\rm sw} V_{\rm sw}/\dot{M}_{\rm fw} V_{\rm fw}$ is the ratio of momentum input in the slow wind to that in the fast wind.

The velocity of the shell is $U_s = (1+\sqrt{\alpha}) v_{\rm sw}$. The aspect ratio, $e = r_{s,E}/r_{s,P}$, is found from the above relation for r_s: $e = (1+\sqrt{\alpha})/(1 + \sqrt{q\alpha})$, where $q = \alpha_E/\alpha_P$.

Bubble geometry.—To use the CTTR model, we must know the angle of incidence θ_i of the converging stream as well as its velocity (see CTTR's Fig. 1). For the proto-PN problem, the angle of incidence must be determined from the aspect ratio by first assuming a shape for the bubble.

Here we assume an elliptical bubble geometry and find the latitude ($\theta_{\rm max}$) at which the refracted postshock wind velocity obtains a maximum ($V_{\rm max}$). Once we have determined $\theta_{\rm max}$, the angle of incidence of the converging stream θ_i can be determined simply by geometry. While this approach is ad hoc, it has the virtues of determining both $V_{\rm max}$ and θ_i self-consistently and of producing results that are in accord with intuition concerning the degree of asphericity in the bubble and its effectiveness in collimating the jets.

To find $\theta_{\rm max}$, we use the results of Icke 1988, who provided details of the flow behind an elliptical inner shock. We first need the angle β between the radius vector for the ellipse, $r(\theta)$, and the ellipse's local tangent; $\beta(\theta)$ can then be fed into the oblique shock relations to find the postshock velocity components parallel and tangential to the elliptical shock. Using relations from Icke's paper, we can determine the angle $\theta_{\rm max}$ where the total postshock velocity $V_{\rm ps} = (v_p^2 + v_\pm^2)^{1/2}$ achieves a maximum. Setting $dv_{\rm ps}/d\theta = 0$ and solving for $\theta_{\rm max}$, we find

$$\theta_{\rm max} = \sin^{-1}\left(\frac{e}{\sqrt{1+e^2}}\right),$$
$$V_{\rm max} = V_{\rm ps}(\theta_{\rm max}) = V_{\rm fw}\sqrt{\left[1 - \frac{16e^2}{(1+e^2)^2}\frac{\gamma}{(\gamma+1)^2}\right]}, \tag{2}$$

where γ is the adiabatic index of the gas and e is the "ellipicity" of the ellipse ($r_{s,E}/r_{s,P}$). In what follows, we use $\gamma = 1.1$, which approximates strong cooling behind the shock.

We consider the tangent to the ellipse at $\theta_{\rm max}$ to determine the angle of incidence. This can be found from simple geometrical considerations, i.e.,

$$\theta_i = \tan^{-1}\left[\frac{e^2}{\tan(\theta_{\rm max})}\right]. \tag{3}$$

After some algebra, it can be shown that $\theta_i = \theta_{\rm max}$. Equations (2) and (3) show that, as the aspect ratio e increases and the bubble becomes more spherical, $\theta_{\rm max}$ and θ_i approach 45°. The effectiveness of CTTR's mechanism decreases as θ_i increases. Equation (3) shows that more spherical bubbles produce larger values of θ_i, which in turn make for less effective jet formation. In addition, as the bubble becomes more spherical, the maximum value of $V_{\rm ps}$ decreases. Lower postshock velocities are less effective at producing jets. Thus, our approach accords with expectations in terms of how effective differently shaped bubbles should be at utilizing CTTR's jet production mechanism.

Jet formation and properties.—We now use the relations derived by CTTR to calculate the time history of jets produced by momentum-conserving proto-PN bubbles. We first convert the wind properties into those for the converging stream (CTTR's Fig. 1). We need the velocity (V_0), mass-loss rate ($\dot{M}_0$), density (ρ_0), and width (y_0) of the converging stream.

The velocity in the converging flow is estimated via $V_0 = V_{\rm max} = V_{\rm ps}(\theta_{\rm max})$ as calculated above. The mass-loss rate into each polar "cone" of the bubble is given by $\dot{M}_0 = \dot{M}_{\rm fw}/2$. The density ρ_0 in the stream is the postshock wind density in the shell ρ_s approximated through ram and the postshock thermal pressure balance in the bubble; $(k/m)T\rho_s = \rho_{\rm wind}(U_s - V_{\rm fw})^2$.

Since U_s is known, we can solve for the shocked wind density in the shell:

$$\rho_s = \left(\frac{m}{kT}\right)\frac{\dot{\Pi}}{4\pi}\left[1-(1+\sqrt{\alpha})\frac{v_{\rm sw}}{v_{\rm fw}}\right] r_s^{-2}. \tag{4}$$

The width y_0 of the annular stream can be found from mass conservation, i.e., $\dot{M}_0 = \pi y_0^2 \rho_0 V_0 \cos\theta_i$. We can now use CTTR's formulae describing the properties of a radiative jet formed by a converging stream, e.g., the jet radius (r_j), density (ρ_j), velocity (v_j), and ram pressure (P_j). Below are CTTR's relations adapted for PPN jets:

$$r_j = \frac{1.29\times10^{-2}}{\sin^2(\theta_i)}\left(\frac{V_{\rm max}}{100\ {\rm km\ s^{-1}}}\right)^2 y_0, \tag{5a}$$

$$\rho_j = 6 \times 10^3 \sin^4(\theta_i)\left(\frac{V_{\max}}{100 \text{ km s}^{-1}}\right)^4 \rho_s , \quad (5b)$$

$$V_j = V_{\max} \cos(\theta_i) , \quad (5c)$$

$$P_j = 6 \times 10^3 \sin^4(\theta_i) \cos^2(\theta_i)\left(\frac{V_{\max}}{100 \text{ km s}^{-1}}\right)^4 \rho_s V_{\max}^2 . \quad (5d)$$

We note that these are the "approximate relations" of CTTR. In the full treatment of the problem, there exists a critical angle of incidence θ_{ic} above which no shock can form and hence no jet will be produced. For a radiative shock, we assume a postshock temperature of $T = 10{,}000$ K, which makes θ_{ic} dependent only on the velocity in the conical flow. An examination of the equations that determine θ_{ic} reveal that no solution exists for $V_{\max} < 20$ km s^{-1}. Thus, if our prolate bubble cannot produce a postshock velocity greater than 20 km s^{-1}, a jet cannot form.

3. RESULTS

In computing predictions from the model, we use the following input parameters: as in KB, we take the initial fast-wind parameters in equation (1) to be $V_{fw0} = 30$ km s^{-1} and $\dot{M}_{fw0} = 5 \times 10^{-6}\ M_\odot$ yr^{-1}. For the exponent in the time dependence, we use $n = 2.5$. The choice of n affects only the bubble evolution timescales. For the slow wind, we take $V_{sw} = 10$ km s^{-1} and $\dot{M}_{sw} = 5 \times 10^{-5}\ M_\odot$ yr^{-1}. For the slow-wind equator to pole density contrast, we adopt three values: $q = 10$, 5, and 2, respectively.

In Table 1, we show the relationship between q, the bubble aspect ratio e, and the fractional maximum velocity in the postshock fast wind, $V_f = V_{\max}/V_{fw}$. Table 1 demonstrates that large values of q produce highly elliptical bubbles with fast postshock flows.

In Figure 2, we present plots of r_j, ρ_j, v_j, and P_j as a function of time for all three models. We normalize the ram pressure P_j to the value of the local slow-wind ram pressure $P_{sw} = r_{sw} V_{sw}^2$, where $\rho_{sw}(R) = \dot{M}_{sw}/4\pi R^2 V_{sw}$.

Figure 2 shows that the model recovers many of the observed characteristics of PN ansae. Let us consider the velocity for $q = 10$, which is most effective at producing a jet. As the velocity of the wind increases, the jet velocity also rises, reaching a maximum velocity of 70 km s^{-1}. Most ansae are observed to have velocities between 50 and 100 km s^{-1}.

The jet will not be able to propagate away from the bubble until $P_j/P_{sw} > 1$. Thus, the P_j/P_{sw} plot shows that, at $q = 10$, the ansa would not be able to propagate outward and start forming a jet until about $t = 100$ yr. This corresponds to a velocity in the converging stream of $V_0 = V_{\max} = 40$ km s^{-1}. Thus, the model avoids the region of parameter space where the CTTR jet production model does not apply.

TABLE 1

POLE TO EQUATOR CONTRAST, ASPECT RATIO, ANGLE OF INCIDENCE, AND FRACTIONAL MAXIMUM VELOCITY FOR THREE MODELS

q	e	θ_i (deg)	V_f
10	0.57	29.5	0.52
5	0.70	34.0	0.35
2	0.87	41.0	0.14

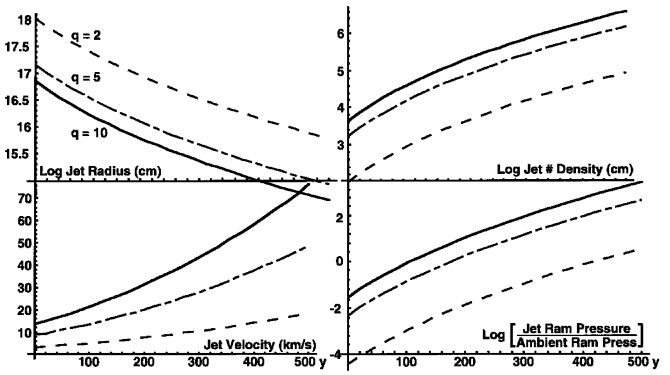

FIG. 2.—The radius, density, velocity, and ram pressure for PPN jets as a function of time. The ram pressure is shown as the ratio of jet to ambient values. Three models with different equator to pole contrasts $q = \rho_E/\rho_P$ are shown in this figure: $q = 10$ (*solid line*); $q = 5$ (*dot-dashed line*); $q = 2$ (*dashed line*). The abscissa shows the time from the end of the superwind. The fast wind begins at $t = 500$ yr.

Next, let us consider the evolution of the radius for $q = 10$ where r_j decreases from $\approx 3 \times 10^{16}$ to $\approx 1 \times 10^{15}$ cm. These values bracket the observed scales for ansae in PNs. The narrowing of the jet with time can explain a puzzling aspect of new *Hubble Space Telescope* (*HST*) images of NGC 6826 (Balick et al. 1996) that reveal the FLIERs to be a series of clumps distributed in a conical zone with its vertex facing the star. Given the narrowing of the base of the jet evident in Figure 2, such a pattern is exactly what our models would predict.

Note that the time dependence of the jet velocity implies that the fast-moving material emitted at the end of the momentum-conserving phase will catch up and sweep up the slower moving gas ejected early on. Depending on the age of a particular PN, one could observe either an extended jet (if the sweeping-up is not complete) or a single clump of material (an ansa) that contains all the jet material.

The $q = 5$ and $q = 2$ models demonstrate the dependence of the jet formation mechanism on the pole to equator contrast. The $q = 5$ case produces an aspect ratio of $e = 0.70$ and only becomes effective at producing a jet ($P_j/P_{sw} > 1$) at later times. The $q = 2$ case produces a nearly spherical bubble with $e = 0.87$ and can just barely produce a jet at the end of the momentum-conserving phase. The jets formed in these cases also have lower densities and velocities than the $q = 10$ case.

The models produce large jet densities ($>10^6$ cm^{-3}) that make it quite likely that the ansae and/or jet will withstand the heating and ionization of stellar UV photons far longer than the nebula that surrounds them. That may account for the low ionizations that are observed. Also, the locally high rate of recombinations will help to maintain a relatively low state of overall ionization for a sound-crossing time after the gas is ionized.

The present calculations suggest that proto-PNs with high-q geometries can sustain their converging flows best and can make long jets. Images of PNs support this prediction nicely. NGC 7354 (Balick 1987) and FG 1 (López, Meaburn, & Palmer 1993) are examples of PNs with highly prolate geometries and long jets. Deep images of the very prolate PN NGC 7009 (the Saturn Nebula; G. Jacoby 1996, private communi-

cation) suggest that it may also belong to this class. On the other hand, as a class, round EPNs such as NGC 3242, 6826, and 7662 have mostly stubby FLIERs, as expected.

Finally, we note that many of the salient features of our model have recently been found in new observations of the asymptotic giant branch (AGB) star V Hydrae (Kahane et al. 1996). Observations of CO lines from the circumstellar shell show evidence for a bipolar outflow of large opening angle with a velocity decreasing with distance from star. The speed at the base of the outflow is measured at $\sim$50 km s^{-1}. A cone-shaped, velocity stratified "jet" with speeds of order 50 km s^{-1} constitutes an explicit prediction of our model, and we consider V Hydrae to be a promising candidate for future detailed comparisons between theory and observations.

4. CONCLUSIONS

The present computations show that the formation of structure in PNs may begin very early in their lifetimes—far earlier than all previous ISW models have assumed. At the very least, the energy-conserving evolution could begin with a pair of dense-walled cavities already in place. In other words, the fast winds that come later might burnish, sculpt, and modify an ambient and highly axisymmetric density distribution.

If this is true, then it is inevitable that the use of one value of q under all sets of circumstances is a gross oversimplification. If a disk like that seen by the *HST* in the Egg Nebula (Sahai, Trauger, & Evans) is a common occurrence, then q may be very high initially. Once the nebula is heated by ionizing stellar radiation, q may decrease as the sound speed of the AGB disk rises suddenly by an order of magnitude. In turn, this means that the structure of PNs is basically set soon after its AGB evolution, and as the wind speeds increase, only some final touches are imposed on its overall shape.

Another possibility is that q is a function of radius and is larger close to the star. Such a radial dependence of the equator to pole contrast $q = q(R)$ is, in principle, what common envelope binary evolution models predict (e.g., Livio 1996). Then, as the bubble expands, it continually "sees" lower values of q and becomes more spherical with time. In this scenario, the evolution of the slow-wind geometry would be imprinted in the PN via the presence and properties of jets and ansae.

The model proposed here could fit into the general explanation of point-symmetric structures suggested by Livio & Pringle (1996) if the slow-wind torus (or accretion disk) were precessing. In our model, a precessing torus would naturally lead to precessing jets (Cliffe et al. 1995). FG 1, Frosty Leo, and the Saturn Nebula show intriguing hints at this possibility in point-symmetric structures imprinted in both ansae and elliptical shells.

In general, the ways in which PNs develop their structure in the proto-PN and standard PN eras of their lives is an important question for the future, and the model outlined here constitutes a first attempt to furnish a more complete theory of PPN evolution. Clearly more work needs to be done.

We thank Garrelt Mellema for his critical insights into the PN jets. A. F. gratefully acknowledges the support of the Minnesota Supercomputer Institute and a Hubble Fellowship (through NASA grant HS-01070.01-94A from the Space Telescope Science Institute, which is operated by AURA, Inc., under NASA contract NASA-26555). B. B. gratefully acknowledges the support of NSF grant AST-917112. M. L. acknowledges support from NASA grant NAGW-2678.

REFERENCES

Aller, L. H. 1941, ApJ, 93, 236
Balick, B. 1987, AJ, 94, 671
Balick, B., Hajian, A., Terzian, Y., Perinotto, M., & Patriarchi, P. 1996, in preparation
Balick, B., Perinotto, M., Maccioni, A., Terzian, Y., & Hajian, A. 1994, ApJ, 424, 800
Balick, B., Preston, H., & Icke, V. 1987, AJ, 94, 164
Balick, B., Rugers, M., Terzian, Y., & Chengalur, J. N. 1993, ApJ, 411, 778
Cantò, J., Tenorio-Tagle, G., & Różyczka, M. 1988, A&A, 192, 287 (CTTR)
Cliffe, J. A., Frank, A., Livio, M., & Jones, J. 1995, ApJ, 44, L49
Dwarkadas, V. V., Chevialier, R. A., Blondin, J. M. 1996, ApJ, 457, 773
Dyson, J. E., & Williams, D. 1980, The Physics of the Interstellar Medium (New York: Wiley)
Frank, A. 1994, AJ, 107, 534
Frank, A., Balick, B., Mellema, G., & Icke, V. 1993, ApJ, 404, L25
Frank, A., & Mellema, G. 1994, ApJ, 430, 800
Icke, V. 1988, A&A, 202, 177
Icke, V., Balick, B., & Frank, A. 1992, A&A, 253, 224
Kahane, C., Audious, P., Barnbaum, C., & Morris, M. 1996, A&A, in press
Kahn, F. D. 1983, in IAU Symp. 103, Planetary Nebulae, ed. D. R. Flower (Dordrecht: Reidel), 305
Kahn, F. D., & Breitschwert, D. 1990, MNRAS, 242, 505 (KB)
Kwok, S., Purton, C. R., & Fitzgerald, M. P. 1978, ApJ, 219, L125
Livio, M. 1996, in Evolutionary Processes in Binary Stars, ed. R. A. M. J. Wijers (Dordrecht: Kluwer), in press
Livio, M., & Pringle, J. E. 1996, ApJ Lett., in press
López, J. A., Meaburn, J., & Palmer, J. W. 1993, ApJ, 415, L137
Marten, H., & Schonberner, D. 1991, A&A, 248, 590
Mellema, G. 1994, A&A, 290, 915
Mellema, G., 1996, preprint
Mellema, G., Eulderink, F., & Icke, V. 1991, A&A, 252, 718
Mellema, G., & Frank, A. 1996, in preparation
Roddier, F., Roddier, C., Graves, J. E., & Northcott, M. J. 1995, ApJ, 443, 249
Sahai, R., Trauger, J. T., & Evans, R. W. 1995, BAAS, 187, 440
Tenorio-Tagle, G., Cantò, J., & Różyczka, M. 1988, A&A, 202, 256